ACS APPLIED MATERIALS & INTERFACES

Letter

www.acsami.org

Low-Temperature Solution-Processed Flexible Solar Cells Based on (In,Ga)N Nanocubes

M. A. Qaeed,[†,‡] K. Ibrahim,[†] K. M. A. Saron,[†,§] M. A. Ahmed,[†] and Nageh K. Allam*[,⊥]

[†]Nano-Optoelectronics Research and Technology Laboratory, School of Physics, Universiti Sains Malaysia, 11800 Penang, Malaysia

[⊥]Energy Materials Laboratory (EML), Department of Physics, School of Sciences and Engineering, The American University in Cairo, New Cairo 11835, Egypt

Supporting Information

ABSTRACT: Indium gallium nitride nanocubes were synthesized via a low-temperature chemical route. Energy-dispersive X-ray spectroscopy and X-ray diffraction analyses confirmed the successful fabrication of (In,Ga)N with various indium mole fractions. The bandgap of the material was tunded as a function of the indium content. The fabricated nanocubes showed a deep level photoluminescence emission at 734 nm as well as in the visible region at 435−520 nm. The Hall effect measurements showed the hole concentration to constantly increase from 6.2×10^{16} to 2.3×10^{18} cm^{-3}, while the hole mobility to decrease from 0.92 to 0.1 $cm^2/(V\ s)$ as the doping ratio increases from 0.005 to 0.025 cm^{-3}. The solar cell device made of nanocubes film containing 0.4 indium on flexible substrates showed a short-circuit current density of 12.47 mA/cm^2 and an open-circuit voltage (V_{oc}) of 0.48 V with 54% fill factor. The relationship between V_{oc} and indium content in the fabricated films was also investigated.

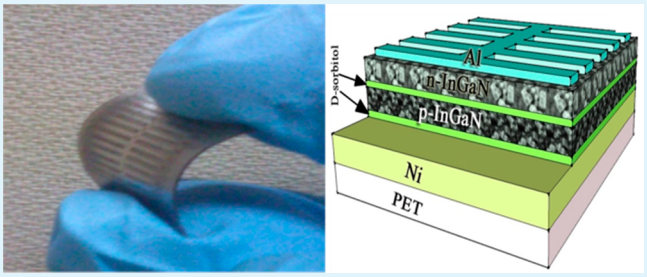

KEYWORDS: *(In,Ga)N, Hall measurements, flexible, solar cell, mobility, low temperature*

Because of their superior physical and chemical properties, III-nitrides have recently shown a great utility in electronic and optoelectronic applications.[1] Among the III-nitride compound semiconductors, the InGaN ternary alloy system has drawn a lot of interest because its direct band gap that can be tunded from 3.4 eV for GaN to 0.7 eV for InN. Consequently, InGaN can be a suitable candidate for the design of high-efficiency optoelectronic devices that operate in the IR, visible, and UV regions of the electromagnetic spectrum.[2] Although a plethora of growth methods are frequently being explored to synthesize III-nitrides, including molecular beam epitaxy (MBE)[3] and metal organic chemical vapor deposition (MOCVD),[4] the growth of high quality InGaN is still challenging, mainly due to the large differences in the lattice constants and binding energies of GaN and InN. In this regard, nanostructured InN and GaN have been synthesized by ammonolysis,[5] laser ablation,[6] and numerous other methods[7] from their respective oxides,[8] halides[9] or pure metals.[9,10] However, these methods are proven inappropriate for the synthesis of $In_xGa_{1-x}N$ particles, as they cannot be directly prepared by merely mixing their starting precursors. For instance, the lowest temperature (900 °C) at which GaN particles can be synthesized from the reaction of Ga_2O_3 with ammonia is impractical because InN already decomposes in ammonia atmosphere at lower temperature. Also, InN is generally prepared in the temperature range 600−730 °C via the reaction of In_2O_3 and ammonia.[8] Although several studies have been reported on the synthesis of (Al,Ga)N nanoparticles,[11] only one study on hexagonal $In_{1-x}Ga_xN$ particles has been reported.[12] This can be understood based on the fact that the cubic phase of III-nitrides is a metastable phase. However, because of the relatively narrower bandgap of cubic InGaN that makes it appropriate for light emitting diode (LED) and solar cell applications,[13] further studies and novel fabrication methods are still urgently needed.

In this study, a novel and low temperature chemical route is explored to produce indium galium nitride nanocubes on flexible substrates under atmospheric pressure conditions, which are very difficulte to be produced using conventionally known techniques. In order to achieve this geometry, the ratio of indium added to GaN was controlled, which possibly influenced the resulting energy gap. To examine the potential application of the synthesized nanostctures, they have been used to fabricate flexible solar cell devices.

Scheme 1 illustrates the steps used to fabricate indium galium nitride nanocubes[13−16] and their assembly on flexible substrates. The detailed experimental section can be found in the Supporting Information.

In an attempt to increase the nitrogen content to yield InGaN nanocubes (NCs) with enhanced geometric structures, we added NH_4OH and HNO_3 to the reaction mixture, followed by exposing it to UV light for 30 min. For each targeted composition, III/V ratios were adjusted by controlling the

Received: April 11, 2014
Accepted: June 17, 2014
Published: June 17, 2014

Scheme 1. Fabrication Steps Used for the Synthesis of (In,Ga)N Nanocubes

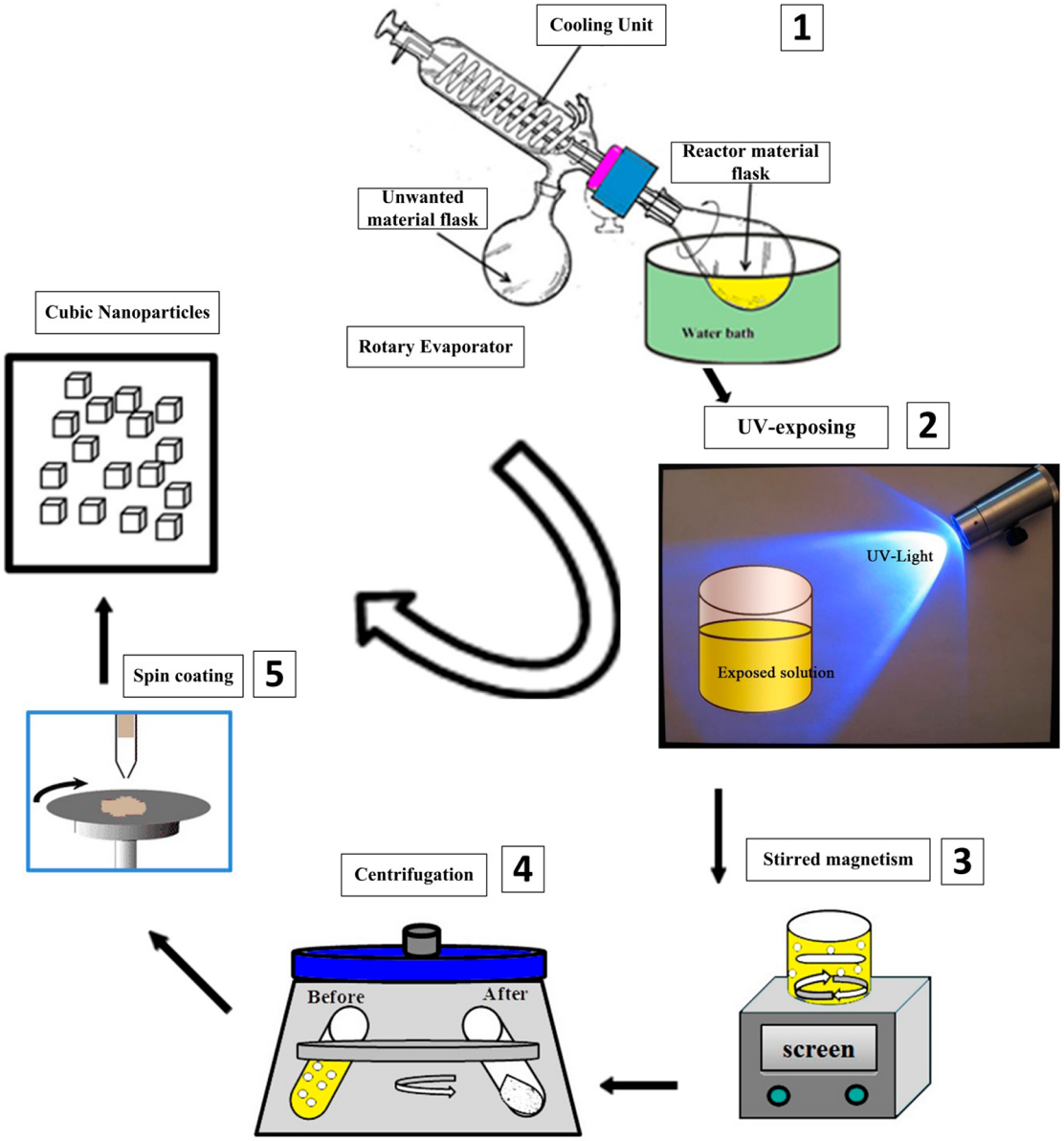

reaction temperature and maintaining the flask cycle times in the water bath at 220 cycle/min. Synthesis times were relatively constant (12 h), and the NCs were typically grown at low temperatures to achieve high indium incorporation. The formation of stable indium can probably be attributed to these temperature and time requirements. Also, observed was the dependence of the NCs density on the ratio of HNO_3/NH_4OH. Higher ratios were found to promote NCs growth, whereas lower ratios resulted in low NCs density.

The InGaN NCs were obtained when HNO_3 and NH_4OH were added to the solution under 90 °C. The experiments demonstrate that the presence of oleylamine is key in providing a strong reducing environment for the thermal decomposition of In $(acac)_3$ and $Ga(acac)_3$. In addition, oleylamine is used as a surfactant to produce nanoparticles of large aggregates with a narrow size distribution. The segregation of nanoparticles is attained by the decomposition of $In(acac)_3$ and $Ga(acac)_3$ in Oleylamine, with some clusters remain present. The success of oleylamine in the preparation InGaN can be attributed to its weak bonding.[17] The results show that the slow growth rate of InGaN in oleylamine, rather than its inherent fast nucleation rate, causes the extended size, suggesting that the dimension of the formed NCs increased with the continuous production of nuclei.

Figure 1 shows FESEM images of the obtained nanostructures, indicating the formation of high density nanocubes. Note that the dimensions of the nanocubes vary with the variation of the In content. The average length of the fabricated nanocubes increases from 90 to 150 nm upon increasing the In mole fraction from 0.2 to 0.4. The size distribution histogram is shown in Figure 1d. In addition, Figure 1e, f shows representitive HR-TEM images, confirming the formation of nanocubes.

The EDX spectra (see the Supporting Information) for the four samples, synthesized with different In fractions (x = 0.1, 0.2, 0.3, and 0.4), showed the existence of In, Ga, N, O, and C. The C and O peaks originate from the PET substrate. The EDX also shows different ratios for In that increase with

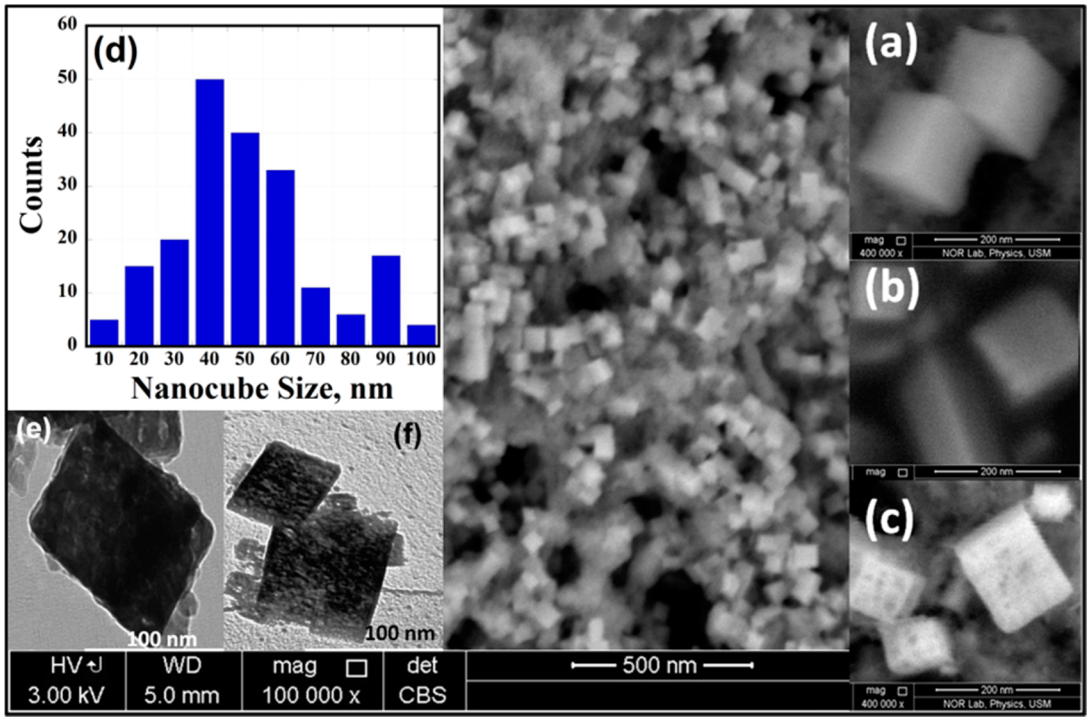

Figure 1. FESEM images of the fabricated (In,Ga)N nanocubes containing (a) 0.2, (b) 0.3, (c) 0.4 indium mole fraction, (d) particle size distrution histogram of the fabricated nanocubes, and (e, f) HR-TEM images showing the formation of nanocubes.

increasing the x fraction, which is also confirmed by XRD measurements. Thermal stability differences between Ga−N and In−N bonds could lead to clustering of indium particles. Therefore, indium-rich clusters were observed during the growth process, possibly as a result of the low temperature used in the experiments.

The InGaN nanocubes were assembled on PET substrates using the drop casting technique. Figure 2a illustrates the XRD patterns of the assembled InGaN nanocubes with different indium mole fractions. The XRD data show the $In_xGa_{(1-x)}N$ to be composed of mixed hexagonal and cubic phases. The thickness of the InGaN film ranges from 500 to 600 nm. The high intensity peak at 2θ = 26° corresponds to the PET substrate,[15,18] whereas the peak at 2θ =31.25° indicates h-InGaN.[15,19] As the In content increases, the $In_xGa_{(1-x)}N$ peaks are shifted from that of GaN toward that of InN. Note the c-InGaN peak at 2θ = 40.28° between InN (200) peak at 39.75° and GaN (220) peak at 40.42° with x = 0.1.[20] Some other peaks of $In_xGa_{(1-x)}N$ can be seen at 40.20, 40.10. and 40.00° with x = 0.4, 0.3, 0.2, and 0.1, respectively, confirming the crystallinity of the $In_xGa_{(1-x)}N$ nanocubes.[20] The In content (x) in $In_xGa_{(1-x)}N$ nanocubes was calculated from the XRD results using the Vegard's law

$$x = \frac{d_{InGaN} - d_{GaN}}{d_{InN} - d_{GaN}} \quad (1)$$

where d_{InGaN}, d_{GaN}, and d_{InN} are interplanar distance parameters of InGaN, GaN and InN, respectively. The average crystallite size of the synthesized nanoparticles (D_P) was calculated using Scherrer's formula,[15] see Table 1.

$$D_P = \frac{0.9\lambda}{\beta \cos\theta} \quad (2)$$

where D_P is the crystal size of nanoparticles, β is the full width at half-maximum (fwhm) of broadened peak, λ is the wavelength of incident X-ray = 0.15406 nm, and θ is the Bragg angle. The $In_xGa_{(1-x)}N$ energy band is calculated from eq 3, where the results are listed in Table 1.

$$E_g(\ln_x Ga_{1-x}N) = E_{GaN} - x(E_{GaN} - E_{InN}) - bx(1 - x) \quad (3)$$

where b (1.43 eV) is the bowing parameter, pertaining the nonlinear fit of band gap energies, x is the indium ratio calculated from eq 1.

In addition to the primary peaks, phase separation is generally recognized as the source of secondary peaks during XRD or PL measurements. This phenomenon minimizes the incidence of primary peaks and improves the material's quality. In this work, the phase separation showed no effect, possibly because the indium ratio is ≤0.6, as well as the higher thickness and the additional gallium species.[21]

The XRD results also show that III sources increase with increasing the growth rate, which further diminishes the phase separation.[22] This result indicates that the structure of the nanocubes is well-established. It can be deduced from the review of previous and contemporary studies that this is the first report showing the shift in XRD peaks of c-InGaN nanostructures synthesized by a chemical method. InGaN-related main diffraction peaks at 40.28, 40.20, 40.10, and 40.00° for samples with x = 0.1, 0.2, 0.3, and 0.4, respectively, were observed. It is evident from the plots that the observed intensity increases with increasing the In fraction in the InGaN/PET samples, which subsequently increases the quality of the material. Also, the diffraction peak shifts to lower 2θ values compared to the bulk values, which can be ascribed to compressive strain in the films.[23] Consequently, the inter planar spacing could be decreased, resulting in the observed increase in the diffraction angle.[18,23]

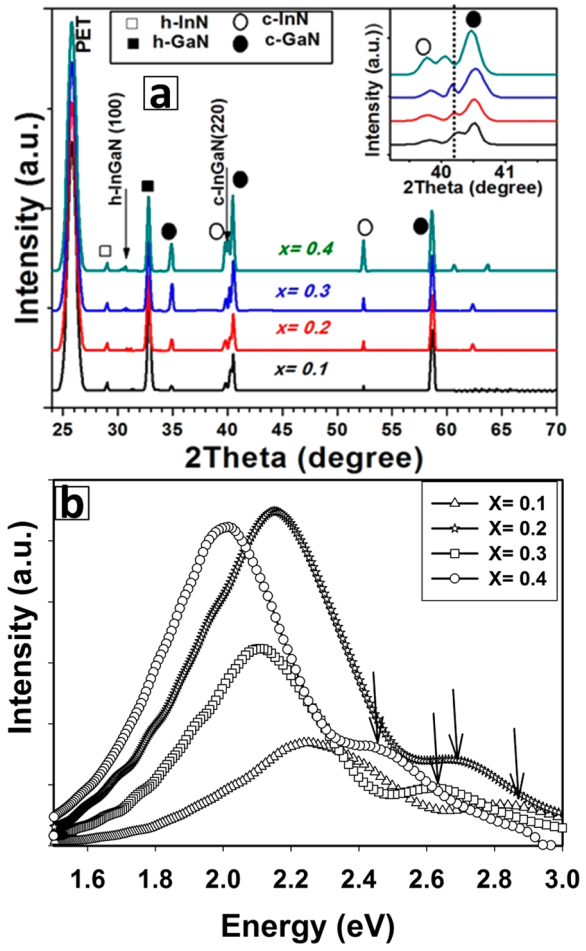

Figure 2. (a) XRD of (In,Ga)N nanostructures deposited on PET substrates and (b) room-temperature photoluminscence spectra of InGaN nanocubes containing different indium mole fractions.

Table 1. Values of the Calculated Indium Content

component	calcd x ratio	2θ	d (Å)	a(Å)	NPs (nm)	energy band (eV)
InN (x = 1)		39.75	2.617	7.402		0.753
GaN (x = 0)		40.42	2.660	7.524		3.211
InGaN1 (x = 0.1)	0.2	40.28	2.651	7.450	9	2.49
InGaN2 (x = 0.2)	0.33	40.20	2.646	7.484	14	2
InGaN3 (x = 0.3)	0.465	40.10	2.640	7.467	16	1.71
InGaN4 (x = 0.4)	0.6	40.00	2.634	7.450	38	1.4

The room temperature photoluminescence (PL) spectra were obtained for the nanocubes containing different indium fractions (x = 0.1, 0.2, 0.3, and 0.4) as depicted in Figure 2b. The tested InGaN nanocubes showed a redshift in the near band edge (NBE) of InGaN, which increases with increasing the indium content. All samples showed a weak peak in the range of 2.9−2.6 eV while other intese peaks appear correspond to emissions from deep levels at yellow band.[24] For all indium fractions, the emission wavelength shifted nonlinearly with increasing the indium mole fraction as a result of increasing complexity of incorporating indium or because of the varying percentage of defects in each case.

In general, the increase of emission can be partly attributed to the indium defects. However, adjusting indium mole fraction limits the increasing high indium content. Therefore, getting an emission at longer wavelengths (green/yellow) in InGaN demands combining the low growth temperature with high indium mole fraction. The increase of emission can also be attributed to the lattice type in the crystal, depending on the composition of the reactive indium through the particle formation process. Therefore, the variations in band gap due to the in-plane tensile stress in InGaN nanocubes can be correlated with the redshift of the PL peak position.[25]

Figure 3a shows the Tauc plots for the drop-casted InGaN nanoparticles on PET substrates, assuming InGaN nanostructures to have direct band gap. The band gaps were found to be 2.94, 2.90 2.82, and 2.69 eV for the samples containing indium fractions of 0.1, 0.2, 0.3, and 0.4, respectively. Similar to the PL spectra, a red-shift in the energy band gap with increasing the indium content was observed, confirming the formation of InGaN nanostructures as InGaN has a slightly larger band gap than that of GaN.[26] However, the InGaN nanocubes prepared with (x = 0.1, 0.2, 0.3, and 0.4) showed band gaps that were red-shifted to lower energy compared to that of bulk c-GaN (3.2 eV).[13,14] The red shift in energy gap can be due to the increase in the crystal intrinsic defects (tensile stress).[25,27] Therefore, the red shift of the band gap of different InGaN

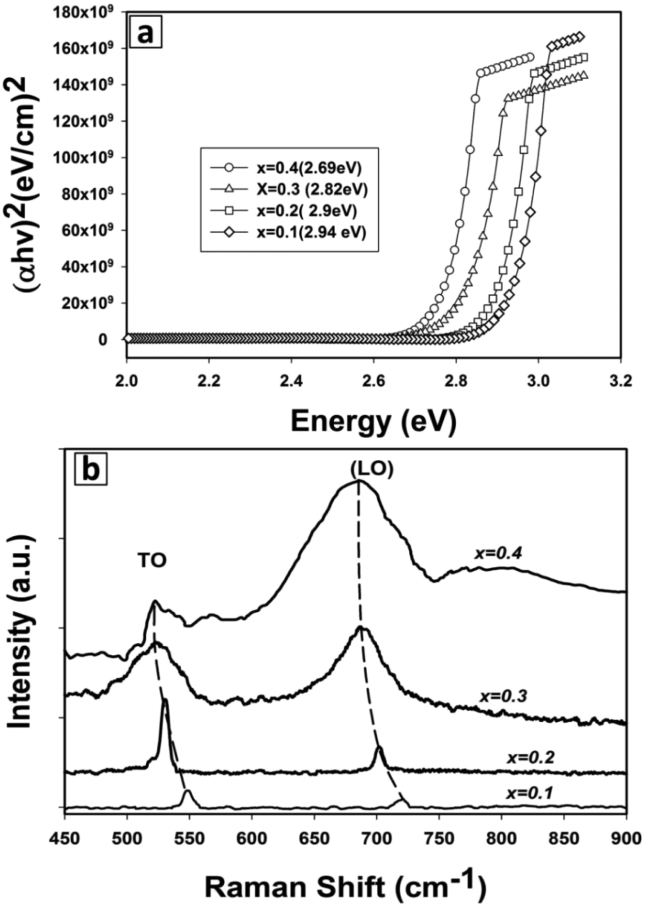

Figure 3. (a) Tauc polts for the (In,Ga)N nanocubes containing different Indium contents and (b) the room-temperature Raman spectra for the InGaN nanocubes containing different indium contents. Raman spectra were acquired using a Jobin-Yvon HR 800 UV system with an Ar ion laser (514.5 nm) excitation source.

dx.doi.org/10.1021/am502217b | ACS Appl. Mater. Interfaces 2014, 6, 9925−9931

nanocubes from 2.95 to 2.65 eV can be attributed to the compositional fluctuation of In.

Figure 3b shows the room-temperature Raman spectra of the InGaN samples containing different fractions of indium ($0.1 \leq x \leq 0.4$). The spectra show peaks corresponding to both the TO and LO high modes of the InGaN alloy. Note that the peaks are down-shifted with increasing the indium content in the material. In the Ga-rich samples, all modes are close to those of bulk GaN (LO) = 733 cm^{-1}, TO = 566 cm^{-1},[18,28] and approach the frequency values of bulk InN, which are A1(LO) = 585 cm^{-1} and TO = 455.7 cm^{-1}.[29] Figure 3b shows that this feature is also shifted to lower frequencies upon increasing the indium content,[28,30] in agreement with the PL and XRD results.

Attaining p-type GaN and AlGaN with high conductivity is a very complex process. This is mainly due to the Mg-acceptor, a commonly used p-type dopant, which has high activation energy (E_a). Studies have shown the intricacy of p-type doping in comparatively high indium content InGaN alloys. This can be attributed to the existence of defects such as nitrogen and/or oxygen vacancies, resulting in high background electron concentrations.[31] The electrical properties of p-type $In_{0.1}Ga_{0.9}N$:Mg alloys at room temperature were plotted as functions of the doping ratio as shown in Figure 4. Noticeable

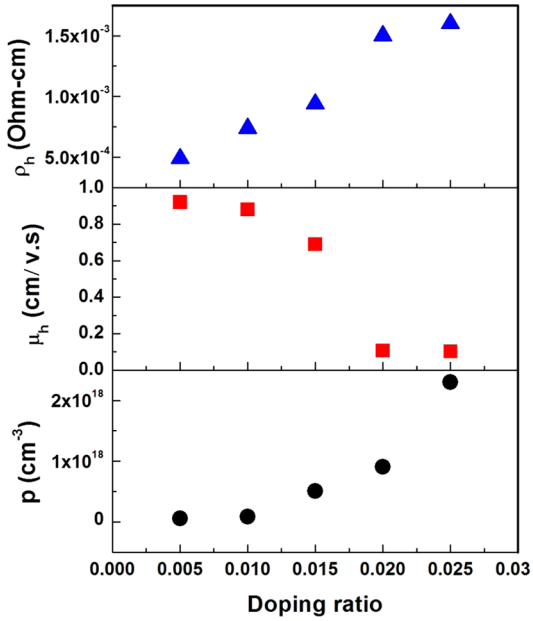

Figure 4. Variation of the hole concentration (p), mobility (μ_h), and resistivity (ρ_h) with doping ratio of p-InGaN films.

changes in mobility and resistivity occurred with increasing the concentration of holes in the samples. The hole's mobility decreases with increasing the concentration of holes, whereas the resistivity increases. It was shown that the hole concentration constantly increases from 6.2×10^{16} (when doping ratio = 0.005) for $In_{0.1}Ga_{0.9}N$ to 2.3×10^{18} cm^{-3} (when doping ratio = 0.25), whereas the hole mobility (μ_h) was found to decrease from 0.92 to 0.1 $cm^2/(V\ s)$ as the doping ratio increases from 0.005 to 0.025.

The dependence of resistivity (ρ) on the doping ratio indicates that ρ increases as the doping ratio increases, reaching a maximum value of 1.6×10^{-3} Ohm cm at a doping ratio of 0.025. This ρ value is among the lowest reported for p-type InGaN prepared by chemical method. The highly obtained μ_h values may reflect the high quality of the material, which leads to lower values of ρ, thereby significantly improving device performance for a plethors of applications. The observed decrease in hole concentration for p-type $In_{0.1}Ga_{0.9}N$, with doping ratio of 5×10^{-3} is a result of hole compensation effect by background electrons.[32]

Figure 5a shows the current−voltage ($I-V$) characteristics for the p-n InGaN nanocube homojunctions. The $I-V$ characteristics of the sample with indium fraction of $x = 0.3$ suggest comparatively larger leakage current (bias-dependent) as compared to the samples with In fractions of $x = 0.1$, 0.2, and 0.4, which affects the overall efficiency of the devices. The leakage current possibly arises during tunnelling by carriers via defect levels, such as V defects and threading dislocations.[33] This is an indication that the density of defects in the sample with indium fraction of $x = 0.3$ is higher than those in the sample containg $x = 0.2$, which is consistent with the decrease of J_{SC}. Recombination currents can also be caused by mechanical scratches, which are widely used as "'model defects"' to study the recombination current produced by extended defects. Comparative analysis based on diamond scratches in ideally behaving cells formed from different loads has also shown the direct relationship between the magnitude of the scratch-induced recombination current and the degree of load-induced disturbance of the crystal.[34]

The efficiency (η) of the fabricated solar cell devices has been estimated from the cell parameters, short circuit current density (J_{SC}), open-circuit voltage (V_{OC}), and fill factor (FF), using eqs 4 and 5[35] and listed in Table 2.

$$\mathrm{FF} = \frac{I_{max}V_{max}}{I_{SC}V_{OC}} \tag{4}$$

$$\eta = \frac{I_{SC}V_{OC}\mathrm{FF}}{P_{in}} \tag{5}$$

The illuminated $J-V$ characteristics of the p-n InGaN/PET homojunction solar cells are shown in Figure 5b, wheras a summary of their relative photovoltaic and electronic parameters is listed in Table 2. The sample containg 0.4 indium mole fraction exhibited the maximum average conversion efficiency of 1.17%. In general, the optimally obtained solar cells showed a 1.19% power-conversion efficiency under 30 mW/cm^2 intensity, which is higher than that reported by heterojunction solar cell grown using MOVPE.[36] This is possibly due to the lower series (R_S) and shunt (R_{sh}) resistances recorded in this work.[37] In this study, the R_s of the devices were obtained following the method proposed in previous studies.[37] The calculated values are also listed in Table 2.

The solar cells fabricated based on $In_{0.4}Ga_{1-0.4}N$ exhibited lower series resistance compared to other samples with lower indium fractions, which should ensure the flow of high current at low applied voltages. Generally, the low series resistance can be related to several factors such as contact resistance, difference of the emitter thickness, doping concentration, and mobility.[37,38] On the basis of our Hall measurements, the lowest series resistance was observed for the sample with $x = 0.4$ with an accompanying higher doping concentration. The sample also exhibited the highest mobility, as it shows the lowest resistivity compared to the other samples. Conversely, higher R_S presented by other samples reflect lower doping concentrations.[38,39] The fabricated p-n InGaN/PET homo-

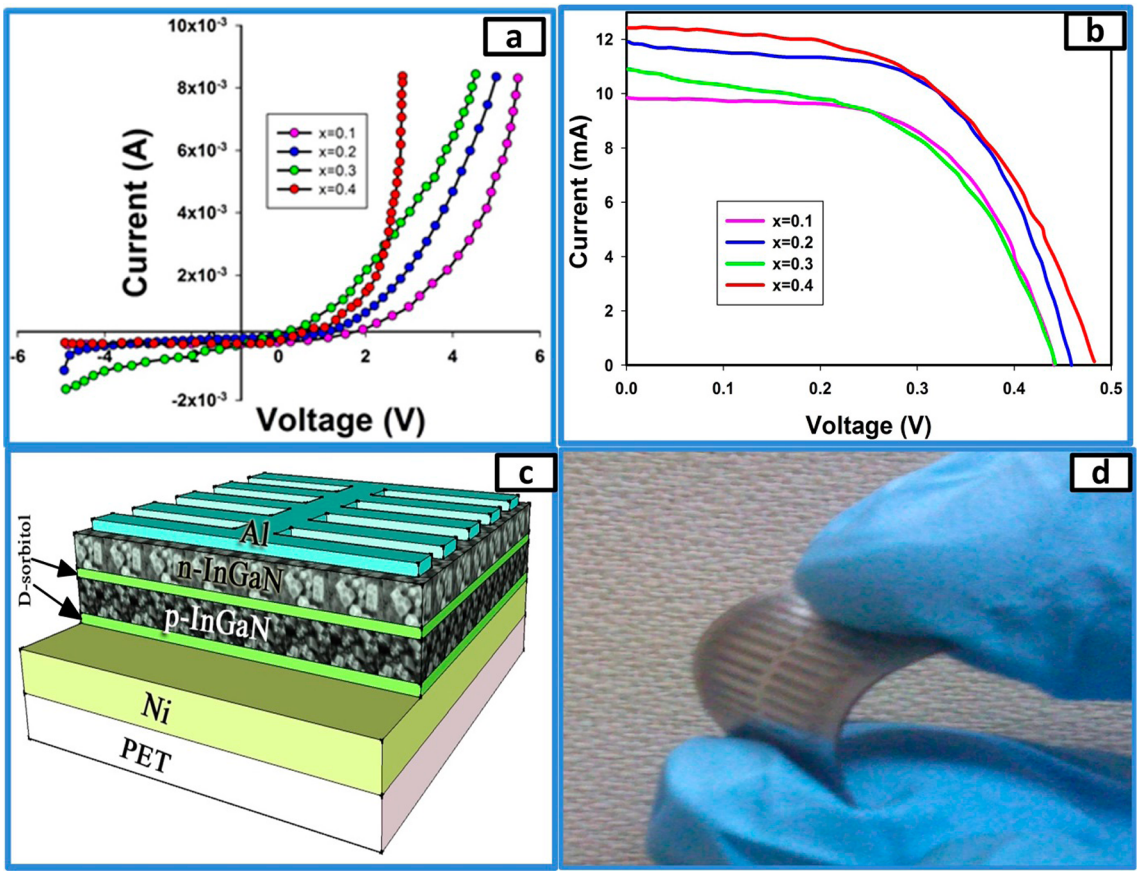

Figure 5. $J-V$ characteristics of the InGaN/PET homojunction solar cells (a) in dark, (b) under solar simulation with power of 30 mW/cm^2, (c) schematic diagram of the fabricated solar cell, and (d) a photo showing the solar cell designed on the flexible substrate.

Table 2. $J-V$ Parameters of the InGaN/PET Homojunction Solar Cells with Different Indium Fractions under Illumination (30 mW/cm^2)[a]

x ratio	V_{oc} (V)	I_{sc} (mA)	V_{max} (V)	I_{max} (mA)	FF	η (%)	R_{series} ($\times 10^{-3}$ Ω)
x = 0.1	0.44	9.9	0.3	8.62	0.59	0.85	84.80
x = 0.2	0.46	11.95	0.31	10.25	0.578	1.06	79.50
x = 0.3	0.44	10.94	0.3	8.62	0.54	0.87	86.00
x = 0.4	0.48	12.45	0.33	10.9	0.6	1.19	71.20

[a]The sample area is 1 cm^2.

junction structure suggests a distinctive model for an InGaN nanostructured films on flixible substrate-based solar cell. This novel approach is an important breakthrough in the development of InGaN-nano particles based full-solar-spectrum photovoltaic success in fabricating InGaN nanoparticles flexible solar cell, Figure 5d.

In conclusion, $In_xGa_{1-x}N$ nanocubes were synthesized by disolving $In(acac)_3$ and $Ga(acac)_3$ in oleylamine at 90 °C. This approach allowed the control of indium content as confirmed by the XRD diffraction spectra, which showed the successful fabrication of InGaN with different In mole fractions without phase separation. FESEM and HR-TEM images clearly indicated the formation of nanocubes. This study is the first to successfully achieve this synthesis in solar cell application. Under simulated solar illumination (30 mW/cm^2), a maximum power conversion efficiency of ∼1.19% was attained for p-n InGaN structures grown on filxible substrate. Ultimately, the results suggest that the low temperature growth of InGaN nanostructures using chemical method can be considered a relatively simple way to synthesize high-performance p-n InGaN/PET single junction solar cell devices. This study also demonstrates the exceptional potential of InGaN nanostructures on PET substrate for use in PV cells.

■ ASSOCIATED CONTENT

Supporting Information

Experimental details and the EDX results. This material is available free of charge via the Internet at http://pubs.acs.org/.

■ AUTHOR INFORMATION

Corresponding Author

*E-mail: nageh.allam@aucegypt.edu.

Present Addresses

‡M.A.Q. is currently at Physics Department, Faculty of Education, Hodeidah University, Al-Hodeidah, Yemen

§K.M.A.S. is currently at Institute of Engineering Research and Materials Technology (IERMT),The National Center for Research, Khartoum 2404, Sudan

Notes

The authors declare no competing financial interest.

■ ACKNOWLEDGMENTS

We thank the Ministry of Higher Education, Malaysia for supporting this work under Grant 203/PSF/6721001. M.A.Q. acknowledges Hodeidah University for awarding him a scholarship to pursue his Ph.D. at USM.

■ REFERENCES

(1) Nakamura, S.; Pearton, S.; Fasol, G. *The Blue Laser Diode: The Complete Story*. Springer: 2000.

(2) Abud, S. H.; Hassan, Z.; Yam, F. Enhancement of Structural and Optical Properties of Porous $In_{0.27}Ga_{0.73}N$ Thin Film Synthesized Using Electrochemical Etching Technique. *Int. J. Electrochem. Sci.* **2012**, *7*, 10038−10046.

(3) Brandt, O.; Sun, Y. J.; Schonherr, H.-P.; Ploog, K. H.; Waltereit, P.; Lim, S.-H.; Speck, J. S. Improved Synthesis of (In,Ga)N/GaN Multiple Quantum Wells by Plasma-Assisted Molecular-Beam Epitaxy. *Appl. Phys. Lett.* **2003**, *83*, 90−92.

(4) Nakamura, S.; Senoh, M.; Nagahama, S. i.; Iwasa, N.; Yamada, T.; Matsushita, T.; Sugimoto, Y.; Kiyoku, H. Room-Temperature Continuous-Wave Operation of InGaN Multi-Quantum-Well Structure Laser Diodes. *Appl. Phys. Lett.* **1996**, *69*, 4056−4058.

(5) Hwang, J.-W.; Campbell, J. P.; Kozubowski, J.; Hanson, S. A.; Evans, J. F.; Gladfelter, W. L. Topochemical Control in the Solid-State Conversion of Cyclotrigallazane Into Nanocrystalline Gallium Nitride. *Chem. Mater.* **1995**, *7*, 517−525.

(6) Tang, T.; Han, S.; Jin, W.; Liu, X.; Li, C.; Zhang, D.; Zhou, C.; Chen, B.; Han, J.; Meyyapan, M. Synthesis and Characterization of Single-Crystal Indium Nitride Nanowires. *J. Mater. Res.* **2004**, *19*, 423−426.

(7) Xiao, J.; Xie, Y.; Tang, R.; Luo, W. Benzene Thermal Conversion to Nanocrystalline Indium Nitride from Sulfide at Low Temperature. *Inorg. Chem.* **2003**, *42*, 107−111.

(8) Schwenzer, B.; Meier, C.; Masala, O.; Seshadri, R.; DenBaars, S. P.; Mishra, U. K. Synthesis of Luminescing (In,Ga)N Nanoparticles from an Inorganic Ammonium Fluoride Precursor. *J. Mater. Chem.* **2005**, *15*, 1891−1895.

(9) Purdy, A. P. Ammonothermal Synthesis of Cubic Gallium Nitride. *Chem. Mater.* **1999**, *11*, 1648−1651.

(10) Balkas, C. M.; Davis, R. F. Synthesis Routes and Characterization of High-Purity, Single-Phase Gallium Nitride Powders. *J. Am. Ceram. Soc.* **1996**, *79*, 2309−2312.

(11) Benaissa, M.; Gonsalves, K.; Rangarajan, S. AlGaN Nanoparticle/Polymer Composite: Synthesis, Optical, and Structural Characterization. *Appl. Phys. Lett.* **1997**, *71*, 3685−3687.

(12) Garcia, R.; Hirata, G.; Farias, M.; McKittrick, J. A Novel Method for the Synthesis of Sub-Microcrystalline Wurtzite-Type $In_xGa_{1-x}N$ Powders. *Mater. Sci. Eng., B* **2002**, *90*, 7−12.

(13) Wu, J. When Group-III Nitrides Go Infrared: New Properties and Perspectives. *J. Appl. Phys.* **2009**, *106*, 01110.

(14) Gopalakrishnan, M.; Purushothaman, V.; Venkatesh, P. S.; Ramakrishnan, V.; Jeganathan, K. Structural and Optical Properties of GaN and InGaN Nanoparticles by Chemical Co-Precipitation Method. *Mater. Res. Bull.* **2012**, *47*, 3323−3329.

(15) Qaeed, M.; Ibrahim, K.; Srivastava, R.; Ali, M.; Salhin, A. Structural and Optical Characterization of InGaN Nanoparticles Synthesized at Low Temperature. *Mater. Lett.* **2013**, 128−130.

(16) Ouyang, J.; Yang, Y. Conducting Polymer as Transparent Electric Glue. *Adv. Mater.* **2006**, *18*, 2141−44.

(17) Xu, Z.; Shen, C.; Hou, Y.; Gao, H.; Sun, S. Oleylamine as Both Reducing Agent and Stabilizer in a Facile Synthesis of Magnetite Nanoparticles. *Chem. Mater.* **2009**, *21*, 1778−1780.

(18) Qaeed, M.; Ibrahim, K.; Saron, K.; Salhin, A. Optical and Structural Properties of Indium Nitride Nanoparticles Synthesized by Chemical Method at Low Temperature. *Sol. Energy* **2013**, *97*, 614−619.

(19) Kawai, Y.; Ohsuka, S.; Iwaya, M.; Kamiyama, S.; Amano, H.; Akasaki, I. In Thick InGaN Growth on Several Crystal Planes of ZnO Substrate by Metalorganic Vapor Phase Epitaxy. *Proc. SPIE* **2008**, 688904.

(20) Hahn, C.; Zhang, Z.; Fu, A.; Wu, C. H.; Hwang, Y. J.; Gargas, D. J.; Yang, P. Epitaxial Growth of InGaN Nanowire Arrays for Light Emitting Diodes. *ACS Nano* **2011**, *5*, 3970−3976.

(21) Guo, Y.; Liu, X.; Song, H.; Yang, A.; Xu, X.; Zheng, G.; Wei, H.; Yang, S.; Zhu, Q.; Wang, Z. A Study of Indium Incorporation in In-Rich InGaN Grown by MOVPE. *Appl. Surf. Sci.* **2010**, *256*, 3352−3356.

(22) Islam, R.; Kaysir, R.; Islam, J.; Hashimoto, A.; Yamamoto, A. MOVPE Growth of $In_x Ga_{1-x} N$ (x= 0−0.4) and Fabrication of Homo-Junction Solar Cells. *J. Mater. Sci. Technol.* **2012**, *29* (2), 128−136.

(23) Mohanty, B. C.; Jo, Y. H.; Yeon, D. H.; Choi, I. J.; Cho, Y. S. Stress-Induced Anomalous Shift of Optical Band Gap in ZnO:Al Thin Films. *Appl. Phys. Lett.* **2009**, *95*, 062103.

(24) Lyons, J.; Janotti, A.; Van de Walle, C. Carbon Impurities and the Yellow Luminescence in GaN. *Appl. Phys. Lett.* **2010**, *97*, 152108.

(25) Stoica, T.; Meijers, R. J.; Calarco, R.; Richter, T.; Sutter, E.; Lüth, H. Photoluminescence and Intrinsic Properties of MBE-Grown InN Nanowires. *Nano Lett.* **2006**, *6*, 1541−1547.

(26) Komaki, H.; Katayama, R.; Onabe, K.; Ozeki, M.; Ikari, T. Nitrogen Supply Rate Dependence of InGaN Growth Properties, by RF-MBE. *J. Cryst. Growth* **2007**, *305*, 12−18.

(27) Reiss, P.; Protiere, M.; Li, L. Core/Shell Semiconductor Nanocrystals. *Small* **2009**, *5*, 154−168.

(28) Harima, H. Properties of GaN and Related Compounds Studied by Means of Raman Scattering. *J. Phys.: Condens. Matter* **2002**, *14*, R967.

(29) Qaeed, M. A.; Ibrahim, K.; Saron, K. M. A.; Abdullah, Q. N.; Elfadill, N.; Abud, S.; Chahrour, K. The Effective Role of Time in Synthesising InN by Chemical Method at Low Temperature. *J. Mater. Sci.: Mater. Electron* **2014**, *25*, 1376−1380.

(30) Correia, M.; Pereira, S.; Pereira, E.; Frandon, J.; Alves, E. Raman Study of the A 1 (LO) Phonon in Relaxed and Pseudomorphic InGaN Epilayers. *Appl. Phys. Lett.* **2003**, *83*, 4761−4763.

(31) Pantha, B.; Sedhain, A.; Li, J.; Lin, J.; Jiang, H. Electrical and Optical Properties of p-Type InGaN. *Appl. Phys. Lett.* **2009**, *95*, 261904.

(32) Chang, C.-A.; Tang, T.-Y.; Chang, P.-H.; Chen, N.-C.; Liang, C.-T. Magnesium Doping of In-Rich InGaN. *J. Appl. Phys.* **2007**, *46*, 2840.

(33) Balkas, C. M.; Basceri, C.; Davis, R. F. Synthesis and Characterization of High Purity, Single Phase GaN Powder. *Powder Diffr.* **1995**, *10*, 266−268.

(34) Breitenstein, O.; Bauer, J.; Lotnyk, A.; Wagner, J.-M. Defect Induced Non-Ideal Dark I−V Characteristics of Solar Cells. *Superlattices Microstruct.* **2009**, *45*, 182−189.

(35) Saron, K.; Hashim, M.; Allam, N. K. Heteroepitaxial Growth of GaN/Si (111) Junctions in Ammonia-Free Atmosphere: Charge Transport, Optoelectronic, and Photovoltaic Properties. *J. Appl. Phys.* **2013**, *113*, 124304.

(36) Islam, R.; Kaysir, R.; Islam, J.; Hashimoto, A.; Yamamoto, A. MOVPE Growth of $In_xGa_{1-x}N$ (x = 0−0.4) and Fabrication of Homo-Junction Solar Cells. *J. Mater. Sci. Technol.* **2012**, *2*, 128−136.

(37) Wu, M.-H.; Chang, S.-P.; Liao, W.-Y.; Chu, M.-T.; Chang, S.-J. Efficiency of GaN/InGaN Double-Heterojunction Photovoltaic Cells Under Concentrated Illumination. *Surf. Coat. Technol.* **2013**, *231*, 253−256.

(38) Tseng, C.-Y.; Lee, C.-T. Improved Performance Mechanism of III−V Compound Triple-Junction Solar Cell Using Hybrid Electrode Structure. *Sol. Energy* **2013**, *89*, 17−22.

(39) Doria, R. T.; Trevisol, R.; de Souza, M.; Pavanello, M. A. Impact of the Series Resistance in the IV Characteristics of Junctionless Nanowire Transistors and its Dependence on the Temperature. *J. Integr. Circuits Syst.* **2012**, *7*, 121−129.